Check for updates

JGR Oceans

RESEARCH ARTICLE
10.1029/2022JC018859

Carbon to Nitrogen Uptake Ratios Observed Across the Southern Ocean by the SOCCOM Profiling Float Array

Kenneth S. Johnson[1], Matthew R. Mazloff[2], Mariana B. Bif[1], Yuichiro Takeshita[1], Hans W. Jannasch[1], Tanya L. Maurer[1], Joshua N. Plant[1], Ariane Verdy[2], Peter M. Walz[1], Stephen C. Riser[3], and Lynne D. Talley[2]

[1]Monterey Bay Aquarium Research Institute, Moss Landing, CA, USA, [2]Scripps Institution of Oceanography, University of California San Diego, La Jolla, CA, USA, [3]School of Oceanography, University of Washington, Seattle, WA, USA

Abstract Measurements of pH and nitrate from the Southern Ocean Carbon and Climate Observations and Modeling array of profiling floats were used to assess the ratios of dissolved inorganic carbon (DIC) and nitrate (NO_3) uptake during the spring to summer bloom period throughout the Southern Ocean. Two hundred and forty-three bloom periods were observed by 115 floats from 30°S to 70°S. Similar calculations were made using the Takahashi surface DIC and nitrate climatology. To separate the effects of atmospheric CO_2 exchange and mixing from phytoplankton uptake, the ratios of changes in DIC to nitrate of surface waters ($\Delta DIC/\Delta NO_3$) were computed in the Biogeochemical Southern Ocean State Estimate (B-SOSE) model. Phytoplankton uptake of DIC and nitrate are fixed in B-SOSE at the Redfield Ratio (RR; 6.6 mol C/mol N). Deviations in the B-SOSE $\Delta DIC/\Delta NO_3$ must be due to non-biological effects of CO_2 gas exchange and mixing. $\Delta DIC/\Delta NO_3$ values observed by floats and in the Takahashi climatology were corrected for the non-biological effects using B-SOSE. The corrected, in situ biological uptake ratio (C:N) occurs at values similar to the RR, with two major exceptions. North of 40°S biological DIC uptake is observed with little or no change in nitrate giving high C:N. In the latitude band at 55°S, the Takahashi data give a low C:N value, while floats are high. This may be due to a change in CO_2 air-sea exchange in this region from uptake during the Takahashi reference year of 2005 to outgassing of CO_2 during the years sampled by floats.

Plain Language Summary Phytoplankton take up dissolved inorganic carbon (DIC) and nitrate as they grow. This results in a decrease in DIC and nitrate during the spring through summer bloom periods each year. The ratio of DIC to nitrate uptake is typically near 6.6 mol C/mol N, a value termed the Redfield Ratio (RR). Here, we used sensor data from an array of profiling floats deployed by the Southern Ocean Carbon and Climate Observations and Modeling program in the Southern Ocean to examine the ratio of C:N uptake by phytoplankton during 243 bloom periods from October through February. We find uptake occurred at values near the RR throughout the Southern Ocean, with two exceptions. North of 40°S, C:N ratios exceed the Redfield value, most likely due to phytoplankton production of a gel-like organic matter deficient in nitrogen. Near 55°S in the Antarctic Southern Zone, an apparent increase in the C:N ratio over the past decade may reflect a change from an air-sea flux of CO_2 into the ocean to a flux out of the ocean.

Key Points:

- Carbon:nitrate uptake ratios by phytoplankton are near the Redfield Ratio in Southern Ocean waters south of 40°S
- Carbon:nitrate uptake ratios north of 40°S are much higher, likely due to production of dissolved organic matter with little nitrogen
- A change in air-sea CO_2 flux during October to February from a sink in 2005 to a source in recent years may have occurred near 55°S

Supporting Information:

Supporting Information may be found in the online version of this article.

Correspondence to:

K. S. Johnson,
johnson@mbari.org

Citation:

Johnson, K. S., Mazloff, M. R., Bif, M. B., Takeshita, Y., Jannasch, H. W., Maurer, T. L., et al. (2022). Carbon to nitrogen uptake ratios observed across the Southern Ocean by the SOCCOM profiling float array. *Journal of Geophysical Research: Oceans*, *127*, e2022JC018859. https://doi.org/10.1029/2022JC018859

Received 16 MAY 2022
Accepted 16 AUG 2022

Author Contributions:

Conceptualization: Kenneth S. Johnson
Data curation: Matthew R. Mazloff, Tanya L. Maurer, Joshua N. Plant, Ariane Verdy
Formal analysis: Kenneth S. Johnson, Matthew R. Mazloff
Funding acquisition: Kenneth S. Johnson, Stephen C. Riser, Lynne D. Talley
Investigation: Kenneth S. Johnson, Matthew R. Mazloff

© 2022. The Authors.
This is an open access article under the terms of the Creative Commons Attribution License, which permits use, distribution and reproduction in any medium, provided the original work is properly cited.

1. Introduction

The cycles of carbon and nitrogen in the ocean are closely linked through the production and remineralization of organic matter that contains both elements in relatively constant proportions. The apparent consistency of this ratio was first identified by Redfield (1934). This observation has become a central tenet of ocean biogeochemistry and is known as the Redfield Ratio (RR). However, it is also clear that biogeochemical processes may act to alter the C:N:P:O_2 ratios from the values suggested by Redfield (Johnson, 2010; Martz et al., 2014). Variations in this elemental stoichiometry may have a profound influence on ocean productivity, and the biological carbon pump (Passow and Carlson, 2012). Here, we are concerned with C and N only, and refer to a molar ratio of 106 C:16 N (6.6:1) as the RR. The ratio of DIC to nitrate assimilated by phytoplankton at any particular location is referred to as C:N. The ratio of DIC to nitrate concentration changes during plankton blooms ($\Delta DIC/\Delta NO_3$) may deviate from C:N due to CO_2 gas exchange, or mixing of waters with different DIC and nitrate ratios during the bloom period.

Methodology: Kenneth S. Johnson, Yuichiro Takeshita, Hans W. Jannasch, Peter M. Walz
Project Administration: Kenneth S. Johnson, Matthew R. Mazloff, Yuichiro Takeshita, Stephen C. Riser, Lynne D. Talley
Software: Matthew R. Mazloff, Tanya L. Maurer, Joshua N. Plant, Ariane Verdy

The stoichiometry of C:N in marine biogeochemical cycles has been the focus of numerous studies following Redfield (1934). This work has ranged from assessments of elemental ratios that are derived from the distribution of dissolved, inorganic constituents within subsurface waters (Anderson & Sarmiento, 1994; Takahashi et al., 1985) to global scale surveys of particle composition in the upper ocean (Copin-Montegut & Copin-Montegut, 1983, Martiny, Pham, et al., 2013; Martiny, Vrugt, et al., 2013). The C:N:P ratios derived from these studies, particularly those focused on particle composition, exhibit relatively large variability (Deutsch & Weber, 2012; Lee et al., 2021; Martiny, Pham, et al., 2013). As noted by DeVries (2018), "In the nutrient-starved subtropical gyres, organic matter C:N:P ratios were as high as 226:37:1, whereas in nutrient rich high-latitude regions they were as low as 66:11:1." The variability in these ratios is driven primarily by the amount of phosphorous in particles. Within the values cited by DeVries, C:N changes from only 6.1:1 to 6.0:1. This relative constancy in C:N is found repeatedly (Anderson & Sarmiento, 1994; Copin-Montegut & Copin-Montegut, 1983; Körtzinger, Hedges, et al., 2001; Martiny, Vrugt, et al., 2013). While the absolute values of the C:N ratio may differ slightly in these studies due to differences in the method used to assess the ratio, the relative variability within each study is low.

As a counterpoint to studies of dissolved chemicals in subsurface waters or studies of particles near the surface, both of which show relatively constant C:N values, several studies have identified significant changes in C:N from changes of dissolved inorganic carbon (DIC) and nitrate (NO_3) concentrations ($\Delta DIC/\Delta NO_3$) in surface waters during bloom periods (Körtzinger, Koeve, et al., 2001, 2008; Sambrotto et al., 1993). Such results have led to the concept of "carbon overconsumption" (Körtzinger, Hedges, et al., 2001; Toggweiler, 1993), which is characterized by C:N > RR. Such carbon overconsumption may be a strategy used by phytoplankton to dissipate photochemical energy, particularly when nutrient stressed (Carlson & Hansell, 2015 and references therein). Measurements of elemental ratios in phytoplankton groups separated by cell sorting also show that photosynthetic bacteria such as *Prochlorococcus* and *Synechococcus* may have C:N values higher than Redfield (Lomas et al., 2021). Thus, it is not a given that C:N ratio will maintain a relatively constant value throughout the ocean.

In this study, we focus on spatial variability in $\Delta DIC/\Delta NO_3$ values that have been observed during the spring and summer months of the Southern Ocean (October through February) using data collected by the Southern Ocean Carbon and Climate Observations and Modeling (SOCCOM) profiling float array. Prior regional studies in the Southern Ocean show that distinct drawdowns in DIC and nitrate may occur during these months (Arrigo et al., 1999; Ishii et al., 2002; Sweeney et al., 2000). These changes have been used to assess the phytoplankton uptake C:N ratios. The observed changes in DIC may be corrected for air-sea gas exchange in these studies (Sweeney et al., 2000), but accurate correction for mixing or advective transport processes is a challenge. Although mixed layers are shoaling during the October to February period, which minimizes the effects of vertical transport on chemical ratios, horizontal transport may be significant. We use the high-resolution Biogeochemical Southern Ocean State Estimate (B-SOSE) model (Verdy and Mazloff, 2017) as a proxy for the transport processes that may influence $\Delta DIC/\Delta NO_3$ and as a tool to correct for the effects of mixing and gas exchange. B-SOSE is a model solution constrained with observations to adjust the initial conditions and atmospheric forcing while still maintaining closed carbon, nutrient, and physical budgets. Our results are then compared to the climatology developed by Takahashi et al. (2014), which includes seasonal cycles of DIC and nitrate. We hypothesize that differences in $\Delta DIC/\Delta NO_3$ from the work conducted by Takahashi et al. (2014) with data nearly two decades old, relative to profiling float observations in the modern ocean, will shed light on possible changes in the air-sea carbon dioxide flux.

2. Materials and Methods

2.1. Profiling Float Measurements

Apex and Navis profiling floats used in this study were deployed as part of the SOCCOM program (Johnson, Plant, Coletti, et al., 2017; Riser et al., 2018). Apex floats were assembled from commercial components at the University of Washington (UW) and Navis floats were purchased as complete units. Nitrate concentrations were measured with ultraviolet optical nitrate sensors, using either the In Situ Ultraviolet Spectrophotometer (ISUS) or the Submersible Ultraviolet Nitrate Analyzer (SUNA) (Johnson et al., 2013). ISUS sensors were built and calibrated at MBARI. pH was determined with Deep-Sea DuraFET pH sensors (Johnson et al., 2016). Most of the pH sensors for Apex floats were built and calibrated at MBARI, while Navis carried sensors built at Sea-Bird. Quality control procedures that have been described previously (Johnson, Plant, Coletti, et al., 2017; Maurer et al., 2021) were applied to the data to correct for sensor drifts or offsets and to flag erroneous values. Only

21699291, 2022, 9, Downloaded from https://agupubs.onlinelibrary.wiley.com/doi/10.1029/2022JC018859 by Noaa Department Of Commerce, Wiley Online Library on [21/04/2023]. See the Terms and Conditions (https://onlinelibrary.wiley.com/terms-and-conditions) on Wiley Online Library for rules of use; OA articles are governed by the applicable Creative Commons License

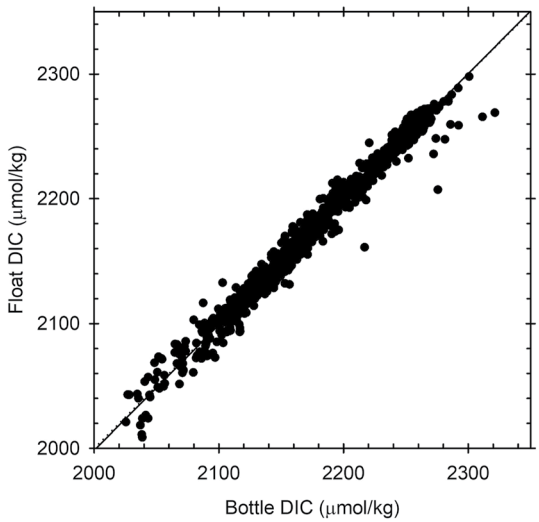

Figure 1. Comparison of DIC computed from float pH and estimated alkalinity on the first float profiles versus DIC measured in samples collected from a hydrographic cast at the float launch. 1,099 pairs have a mean difference of 0.4 ± 8 µmol kg^{-1} (1 SD). Dashed line is the 1:1 relationship and the solid line is a Model II regression.

nitrate and pH data that were flagged as Good were used in this study. After quality control adjustments, the mean sensor nitrate concentration difference from bottle samples collected when floats were launched (n = 2,644) was 0.2 µmol kg^{-1} with a standard deviation of 1 µmol kg^{-1}. The mean sensor pH differed from discrete samples (n = 1,262) by 0.002 with a standard deviation of 0.015 (Maurer et al., 2021).

DIC was then computed from the observed pH and a total alkalinity (TA) that was estimated using both the LIAR v2 algorithm (Carter et al., 2018) and the CANYON-B neural network system (Bittig et al., 2018). Calculations were performed using CO2SYS (Lewis & Wallace, 1998) and equilibrium constants selected in Wanninkhof et al. (2016). The DIC values determined using TA estimates based on LIARv2 and CANYON-B are generally consistent. If the correlation coefficient between the seasonal (October to February) rate of decrease in DIC and nitrate in the upper 30 m for all floats is used as a metric for consistency, both LIAR (R = 0.812) and CANYON-B (R = 0.827) alkalinity estimates perform similarly. With no significant reason to select one method over the other, we have used the mean of the DIC values computed from the alkalinity estimated with each algorithm.

An assessment of the accuracy of the estimated DIC values was made by comparing these values with DIC concentrations measured in hydrocasts at the time floats were deployed (Figure 1). The hydrocast DIC concentrations were directly measured values obtained from data files downloaded from the CLIVAR and Carbon Hydrographic Data Office (CCHDO; cchdo.ucsd.edu). The data from CCHDO were generally collected on GO-SHIP cruises (Talley et al., 2016). In addition, several floats used in the comparison plots were deployed at the Hawaii Ocean Time-series (HOT) program Station Aloha. DIC concentrations for these floats were downloaded from the HOT data server (https://hahana.soest.hawaii.edu/hot/hot-dogs/interface.html). The mean difference between the float estimates of DIC and measured values is less than 1 µmol kg^{-1} with a standard deviation from the regression shown in Figure 1 of 8 µmol kg^{-1}. Some of the 8 µmol kg^{-1} standard deviation arises due to ocean variability in the approximately 18 hr time lag that occurs between hydrocasts at the time of float deployment and completion of the first vertical float profile. We expect that the estimated DIC values have a real standard deviation closer to 5 µmol kg^{-1}, which is consistent with the 4 µmol kg^{-1} estimate of Williams et al. (2018). The only difference between our approach and that of Williams et al. (2018) was our use of a mean alkalinity estimate from Carter et al. (2018) and Bittig et al. (2018). The offset and standard deviation of the DIC derived from float pH are also similar to the values Woosley et al. (2017) reported in a comparison of measured DIC and values derived from pH and TA determined in the same samples. This implies no significant bias in the DIC values during austral spring to fall, when most floats are launched. If the alkalinity has a strong seasonal cycle not captured by either LIAR or CANYON-B, then it is possible that errors in the estimated DIC during October are larger. This is discussed further below. The accuracy of the float pH data does not appear to degrade in time (Johnson, Plant, Coletti, et al., 2017; Maurer et al., 2021), suggesting that the DIC estimates should retain similar accuracy values over time.

Data from the upper 30 m of the water column were used to create the time series. To control for the effects of dilution or ice formation, all concentrations of DIC and nitrate were normalized to a salinity of 35 before analysis (e.g., sDIC = DIC * 35/S) where S is salinity. The salinity normalized concentrations were used in all analyses. In the remainder of the study, DIC and NO_3 will refer to the salinity normalized concentrations. Each austral spring through summer period (October to February) in multi-year records of data from single floats was treated as an independent time series. Additional constraints were then applied to select appropriate time series for analysis. These constraints were as follows: (a) only time series with median positions south of 25°S, (b) time series that began in the months October to December, and (c) more than 2 months of available data. After applying these conditions, 243 seasonal cycles were available for analysis. These seasonal cycles were collected by 115 different profiling floats. Float WMO number and start date for each cycle are listed in Table S1 of the Supporting Information S1 along with position information and a summary of analysis results. Data were binned by 5° of latitude

21699291, 2022, 9, Downloaded from https://agupubs.onlinelibrary.wiley.com/doi/10.1029/2022JC018859 by Noaa Department Of Commerce, Wiley Online Library on [21/04/2023]. See the Terms and Conditions (https://onlinelibrary.wiley.com/terms-and-conditions) on Wiley Online Library for rules of use; OA articles are governed by the applicable Creative Commons License

21699291, 2022, 9, Downloaded from https://agupubs.onlinelibrary.wiley.com/doi/10.1029/2022JC018859 by Noaa Department Of Commerce, Wiley Online Library on [21/04/2023]. See the Terms and Conditions (https://onlinelibrary.wiley.com/terms-and-conditions) on Wiley Online Library for rules of use; OA articles are governed by the applicable Creative Commons License

for several analyses. There were relatively few seasonal cycles in the 70°S bin ($n = 8$), so we have omitted it from the discussion of binned data.

2.2. Takahashi Climatology

In addition to the profiling float data, we also analyzed the climatology prepared by Takahashi et al. (2014). The climatology contains both DIC and nitrate, which enables a comparison with the analysis of float data. The DIC values in the Takahashi climatology were computed from measured pCO_2 and an estimate of TA. They compared calculated DIC values to 2,000 direct DIC measurements made simultaneously with pCO_2. The computed DIC values have a root mean square deviation from direct measurements of ± 3 μmol kg^{-1}. This is somewhat better than the value derived from float data. However, the alkalinity values used with pCO_2 to estimate DIC were directly measured in these comparisons and not estimated as done in this work. Nitrate concentrations in the Takahashi climatology were obtained from monthly gridded surface values in World Ocean Atlas (Conkright et al., 1994).

2.3. B-SOSE Model

In parallel with the profiling float observational data, we use a biogeochemical, data-assimilating model to test various assumptions concerning biases introduced by advection, mixing, gas exchange, and float motion. This product, the Biogeochemical Southern Ocean State Estimate (B-SOSE), is described in Verdy and Mazloff (2017). Recent updates to the model include time period (now running from 2013 to 2018), resolution (now with 1/6° horizontal resolution), and some minor updates to the NBLING biogeochemical component. NBLING is the Nitrogen version of the Biogeochemistry with Light, Iron, Nutrients, and Gases model that has evolved from Galbraith et al. (2010). The major NBLING update is that biomass is now a prognostic variable in the model.

B-SOSE has closed physical and biogeochemical budgets over the 6-year simulation. In this sense, it is a pure model simulation. However, in producing B-SOSE, the initial conditions and atmospheric state are systematically adjusted through an adjoint-based iterative process. The goal is to make the solution as consistent as possible with in situ and satellite measurements, including the float measurements analyzed here. Because the budgets are closed, the model solution lacks controllability (e.g., by nudging), and discrepancies between B-SOSE and the data do exist, especially at the mesoscale. Nevertheless, B-SOSE does provide a baseline estimate of the large-scale Southern Ocean biogeochemistry, sea ice, and physical properties. The solution analyzed here is labeled Iteration 134, and monthly averaged values for temperature, salinity, nitrate, and DIC were interpolated to an approximately 1° resolution grid for analysis in this work. Mixed layer depth is determined by finding the maximum in the second derivative of density (i.e., the location of fastest stratification increase) above the pycnocline. Here the pycnocline is defined as the maximum in the first derivative of density. In B-SOSE, the C:N ratio is fixed at the canonical RR of 6.6.

3. Data Sources

Float data used in this analysis were from the LIAR and CANYON-B low vertical resolution text file products downloaded from the SOCCOM website (https://soccom.princeton.edu) with a Digital Object Identifier doi.org/10.6075/J00R9PJW in December 2021. The low-resolution files contain all of the biogeochemical sensor data, but the high-resolution (2 m) CTD data are decimated to the vertical resolution of the biogeochemical sensors. Additional float profiles through the end of 2021 were also downloaded in this format directly from the SOCCOM website. B-SOSE model output for Iteration 134 was downloaded from http://sose.ucsd.edu/SO6/ITER134/. Decimated data files with monthly and 1° resolution were used for the analyses. The Takahashi et al. (2014) data set used here was downloaded from https://www.ncei.noaa.gov/access/ocean-carbon-data-system/oceans/ndp_094/ndp094.html. This is referred to as the Takahashi climatology in the remainder of the manuscript. Analysis code and B-SOSE output results are available at http://sose.ucsd.edu.

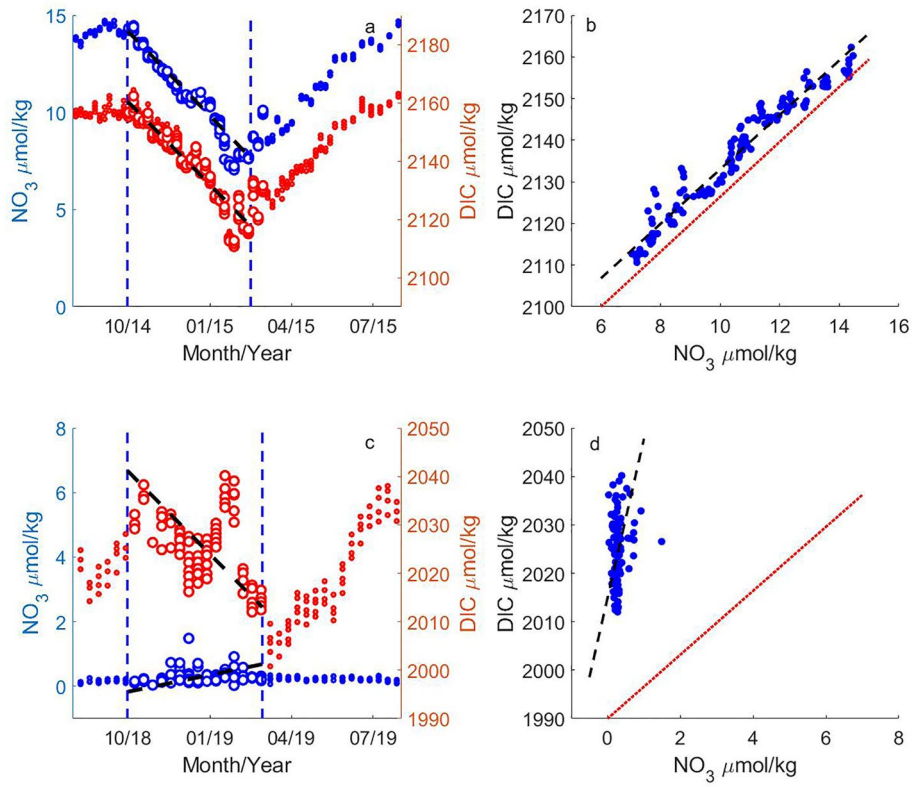

Figure 2. Annual cycles of nitrate and DIC. (a) Annual cycle of nitrate (blue) and DIC (red) using all data in the upper 30 m for float 5,904,188 at 49.5°S (Figure 3). Open circles are data from October through February and dashed lines are least squares fits used to determine $\Delta DIC/\Delta t$ and $\Delta NO_3/\Delta t$. Vertical dashed blue lines delineate the October to February time frame used to determine concentration changes. (b) DIC versus nitrate for the months October through February of the 2014/2015 season in the upper 30 m. The dashed line is a Model II least squares fit. The slope of the Redfield Ratio is shown by the red line through an arbitrary intercept. (c) DIC and nitrate annual cycles as in panel (a) for float 5,904,844 at 29°S (Figure 3). (d) DIC versus nitrate as in panel (b).

4. Results and Discussion

4.1. Seasonal DIC and Nitrate Drawdown

Decreases in the concentrations of nitrate and DIC occur in waters south of about 40°S during the months of October through February as organic matter is produced by the phytoplankton community. Annual cycles of DIC and nitrate from float 5904188 (UW serial number 9095) are shown in Figure 2a to illustrate the seasonal drawdown. The location of the time series is shown in Figure 3. Decreasing concentrations of DIC and nitrate from October through the end of February are clear. These drawdowns allow the ratio of the change in DIC to nitrate concentration ($\Delta DIC/\Delta NO_3$) from October through February to be well constrained. A value of 6.54 ± 0.12 mol C:mol N (1 SD, $R = 0.97$) is obtained for the slope of the data in Figure 2b. All slopes for data with uncertainty in both the X and Y variables were computed using a Model II, geometric mean least squares regression (Laws, 1997).

Clear decreases in DIC concentrations are also apparent in seasonal cycles equatorward of 40°S. However, the nitrate concentrations approach 0 and nitrate concentration has a much smaller seasonal drawdown than expected from the DIC change and the RR. An example is shown in Figure 2c for a seasonal cycle observed by float 5904844 (UW serial number 9766) at 29°S (Figure 3). While DIC decreases about 20 μmol kg^{-1} from October through February, the nitrate concentration detected by float sensors was near 0 and the nitrate data had no significant trend. The slope of a regression fitted to the DIC and nitrate data (Figure 2d) was 32 ± 5 mol C:mol N. Given the small change in nitrate in this region, the $\Delta DIC/\Delta NO_3$ ratios may become very large and, in some cases, negative due to random changes in the low nitrate concentrations at the level of the sensor noise.

21699291, 2022, 9, Downloaded from https://agupubs.onlinelibrary.wiley.com/doi/10.1029/2022JC018859 by Noaa Department Of Commerce, Wiley Online Library on [21/04/2023]. See the Terms and Conditions (https://onlinelibrary.wiley.com/terms-and-conditions) on Wiley Online Library for rules of use; OA articles are governed by the applicable Creative Commons License

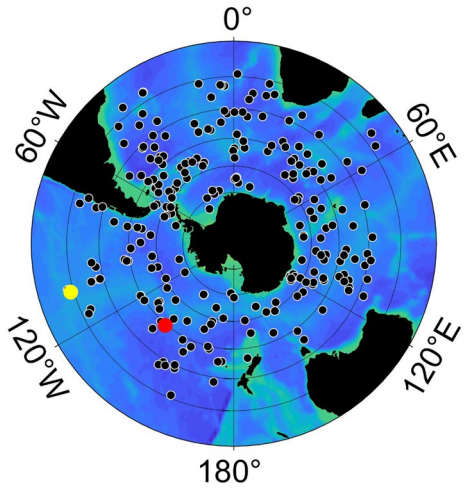

Figure 3. Median locations of the 243 seasonal cycles of float data analyzed here. Red dot is median location (49.56°S, 139.95°W) of float 5904188/9095 seasonal cycle shown in Figure 2a. Yellow dot is median location (29.12°S, 106.52°W) of float 5904844/9766 seasonal cycle shown in Figure 2c. The Subtropical Front, Subantarctic Front, and Southern Antarctic Circumpolar Current Front (Orsi et al., 1995) are shown as red, yellow, and magenta lines. Shading is water depth. The map extends to 20°S with 10° latitude circles.

The 243 seasonal records of DIC and nitrate drawdown in October through February time frame encompass nearly all regions of the Southern Ocean from near 30°S to the continental slope of Antarctica (Figure 3). The rates of change in DIC and nitrate (ΔDIC/Δt and $\Delta NO_3/\Delta t$) were calculated for each of these seasonal cycles from a linear regression of the DIC and nitrate data versus data between October 1 and February 28 in the upper 30 m. The rate of DIC drawdown for each of the 243 cycles is plotted versus the rate of nitrate drawdown in Figure 4a. The rates of DIC and nitrate drawdown are significantly correlated ($R = 0.82$, $P < 0.0001$). The slope of the relationship between the rate of DIC drawdown and nitrate drawdown observed by the floats ($\Delta DIC/\Delta NO_3$) for all of the seasonal cycles (Figure 4a) was 6.6 ± 0.3 mol C:mol N (1 SD).

4.2. DIC to Nitrate Uptake Ratios by Phytoplankton

The $\Delta DIC/\Delta NO_3$ slope of the time series sampled by the floats may differ from the C:N uptake ratio during phytoplankton production due to a variety of processes, including CO_2 gas exchange, mixing and advective processes, or non-Lagrangian sampling produced by the motion of the floats through chemical gradients. To assess the effects of these processes on $\Delta DIC/\Delta NO_3$, an equivalent seasonal time series to each of the 243 float seasonal cycles was sampled in the B-SOSE model domain. Figure 4a shows the rates of DIC change plotted versus the nitrate rates of change that were sampled in B-SOSE at fixed positions that correspond to the median latitude and longitude of each float seasonal cycle. These rates sampled in B-SOSE at a fixed location for each seasonal cycle data set are termed B-SOSE_{MP} for B-SOSE at the median profile position. It is clear that the changes in DIC and nitrate sampled over time at fixed positions in the model have much less variability than the float data, spanning smaller ranges of ΔDIC/Δt and $\Delta NO_3/\Delta t$. Despite less variability, the slope of the least squares fit to the B-SOSE_{MP} dat aset ($\Delta DIC/\Delta NO_3 = 6.8 \pm 0.2$, $R = 0.86$) is similar to the float value.

Figure 4b shows the rates of change of DIC and nitrate concentrations for each of the 243 seasonal cycles that were sampled from B-SOSE at the time and position of each individual float profile, as well as the float values. This data set is termed B-SOSE_{PP} (B-SOSE Profile Position). The range of values in the float and B-SOSE_{PP} data are quite similar in this comparison. Figures 4c and 4d show histograms of the ΔDIC/Δt and $\Delta NO_3/\Delta t$ values observed by the floats and the values sampled in B-SOSE_{PP}. The spread for the two ΔDIC/Δt distributions (1 SD = 0.22 for floats and 0.19 μmol/kg/d for B-SOSE_{PP}) are not statistically different (Brown-Forsythe equal variance test, $p = 0.051$). The float and B-SOSE_{PP} $\Delta NO_3/\Delta t$ data sets have variances that are somewhat similar (1 SD = 0.033 and 0.026 μmol kg^{-1} d^{-1}), but these values are statistically different ($p < 0.05$).

Seasonal errors in the estimated alkalinity could bias the $\Delta DIC/\Delta NO_3$ drawdown ratios. For example, alkalinity changes driven by calcification in the Southern Ocean (Balch et al., 2016) would change the alkalinity on which the ΔDIC values are predicated. Amounts of calcification or other processes having an important effect on the DIC estimates would manifest through a seasonal change in salinity normalized alkalinity (sTA = TA * 35/S). However, observations of alkalinity from coastal regions (Arroyo et al., 2020) to open waters (Brix et al., 2013; Louanchi et al., 2001; Shadwick et al., 2015) of the Southern Ocean find salinity normalized alkalinity measured throughout the year to be conservative. This suggests that there will be little effect from calcification on the ΔDIC values that are computed from float data. We assume it has little bias on the results.

Profiling float data are often considered to represent sampling in a Lagrangian framework. However, advection at the 1,000 m parking depth decouples the float from surface waters. Analysis in the B-SOSE model allows some assessment of the degree of decoupling. The B-SOSE_{MP} and B-SOSE_{PP} data in Figures 4a and 4b illustrate the difference between data in an Eulerian coordinate system (B-SOSE_{MP}) and the mobile float data (B-SOSE_{PP}). The largest values of ΔDIC/Δt and $\Delta NO_3/\Delta t$ for both floats and B-SOSE_{PP} in Figure 4b result from floats that move large distances, crossing frontal boundaries. This represents non-Lagrangian behavior. In a prior analysis of seasonal changes in surface nitrate (Johnson, Plant, Dunne, et al., 2017), we eliminated cycles where the floats sampled large salinity changes. Here we have opted to retain cycles with large salinity changes to avoid rejecting

21699291, 2022, 9, Downloaded from https://agupubs.onlinelibrary.wiley.com/doi/10.1029/2022JC018859 by Noaa Department Of Commerce, Wiley Online Library on [21/04/2023]. See the Terms and Conditions (https://onlinelibrary.wiley.com/terms-and-conditions) on Wiley Online Library for rules of use; OA articles are governed by the applicable Creative Commons License

21699291, 2022, 9, Downloaded from https://agupubs.onlinelibrary.wiley.com/doi/10.1029/2022JC018859 by Noaa Department Of Commerce, Wiley Online Library on [21/04/2023]. See the Terms and Conditions (https://onlinelibrary.wiley.com/terms-and-conditions) on Wiley Online Library for rules of use; OA articles are governed by the applicable Creative Commons License

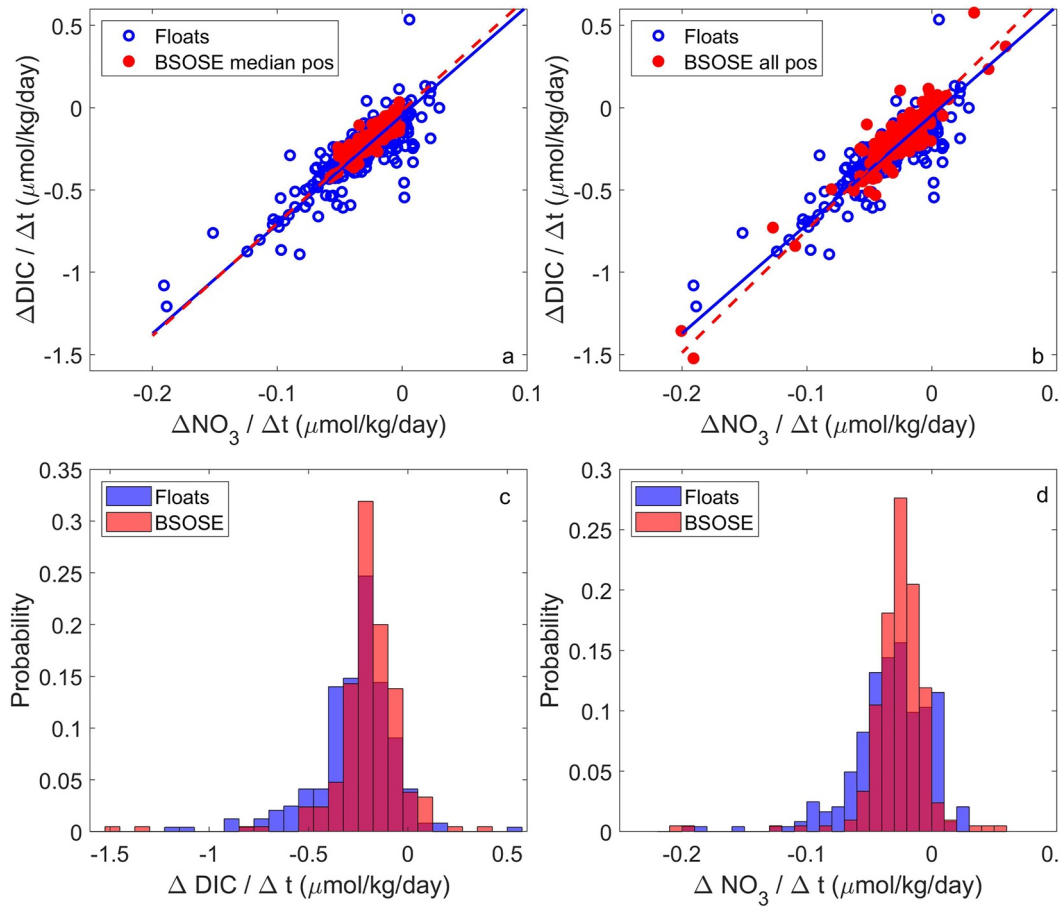

Figure 4. Rates of DIC and nitrate change. (a) Rate of change of DIC in the upper 30 m versus rate of change in nitrate for each of 243 profiling float time series in the months of October through February of 2014 through 2021 (blue circles). Rates of change in B-SOSE sampled at the median latitude and longitude of each float time series (B-SOSE$_{MP}$) in beginning in October 2015 through February 2016 are shown in red. Model II regression lines are shown in blue (floats) and red (B-SOSE$_{MP}$). (b) As in panel (a), but B-SOSE was sampled at the location of each individual float profile (B-SOSE$_{PP}$). (c) Histograms of the 243 rates of change in DIC in the float data (blue) and B-SOSE$_{PP}$ (red). (d) As in panel (b) for nitrate rate of change.

signals in regions with large amounts of ice melt. We use B-SOSE as a tool to correct for any biases that are introduced by the non-Lagrangian behavior of floats.

Given the small differences in the distributions of the float and B-SOSE$_{PP}$ data for ΔDIC/Δt and $\Delta NO_3/\Delta t$, we assume that B-SOSE$_{PP}$ is a good proxy for approximating the effects of transport processes and gas exchange on the float data trends. The slope of the ΔDIC/Δt values versus those for $\Delta NO_3/\Delta t$ in the B-SOSE$_{PP}$ data is $\Delta DIC/\Delta NO_3 = 7.4 \pm 0.2$ (Figure 4b), which was computed using the B-SOSE solution for the year 2015. If we repeat the calculation in B-SOSE for each of the model years with continuous data from October through February (seasons beginning in October 2014 through October 2018), the $\Delta DIC/\Delta NO_3$ values determined from a regression of ΔDIC/Δt on $\Delta NO_3/\Delta t$ range from 6.75 to 7.55 with a mean of 7.2 ± 0.3 (1 SD).

Biological uptake of C and N in B-SOSE are fixed at a ratio RR = 6.6. The slope of the $\Delta DIC/\Delta NO_3$ values sampled in B-SOSE$_{PP}$ (Figure 4b) is higher than the biological uptake ratio by a factor of 7.2/6.6 = 1.09. The difference requires that gas exchange, advection, mixing, and non-Lagrangian motion have biased the results. If the bias multiplier in the B-SOSE$_{PP}$ results is an accurate reflection of a similar bias in the float data in Figure 4b, then the biological uptake ratio of C and N (C:N) was occurring at a ratio of $6.6 \times 6.6/7.2 = 6.0 \pm 0.4$ mol C:mol N in the region sampled by the floats. The error has been computed as the square root of the squared standard deviations of the float and the B-SOSE $\Delta DIC/\Delta NO_3$ slopes. However, the $\Delta DIC/\Delta NO_3$ values in float and B-SOSE$_{PP}$ data determined as the slope in Figure 4b are heavily influenced by the most extreme ΔDIC/Δt

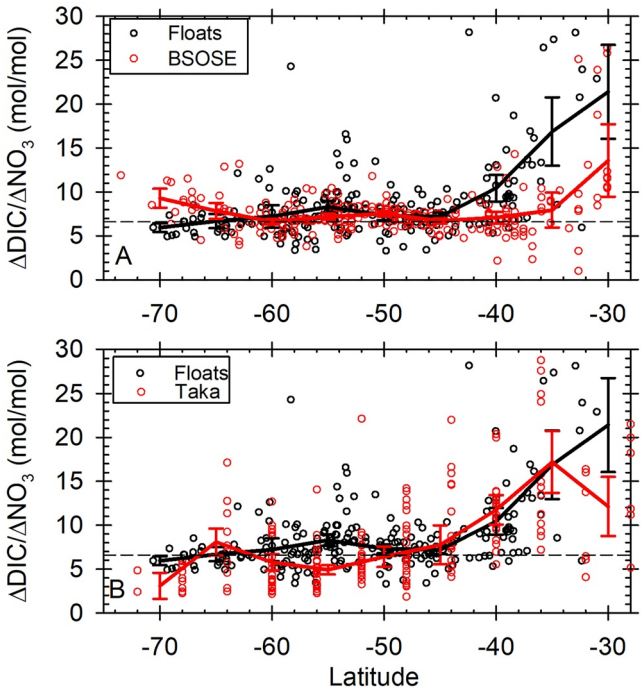

Figure 5. Ratio of DIC to nitrate concentration change versus latitude. (a) $\Delta DIC/\Delta NO_3$ from each of the 243 seasonal drawdown cycles observed by floats (black circles) or B-SOSEPP (red circles) determined from the slope of a regression of DIC on nitrate for each seasonal cycle are plotted versus median latitude of each seasonal cycle. Solid lines connect the mean ±90% CI for 5° bins in latitude. (b) As in panel (a) for floats and the Takahashi data set.

and $\Delta NO_3/\Delta t$ values. The largest negative $\Delta DIC/\Delta t$ and $\Delta NO_3/\Delta t$ values are found in seasonal cycles where the floats go through large latitude changes and sample different surface water masses as noted above. These large $\Delta DIC/\Delta t$ and $\Delta NO_3/\Delta t$ values are more strongly influenced by advection than the typical values.

An alternative approach to assessing $\Delta DIC/\Delta NO_3$ is to compute the values for each individual seasonal cycle from a regression of DIC versus nitrate, as in Figure 2b. The large number of seasonal cycles that are available allow some geographic resolution of the $\Delta DIC/\Delta NO_3$ values determined in this manner. Figure 5 shows the $\Delta DIC/\Delta NO_3$ values versus latitude for each of the 243 time series from floats, B-SOSE, and from the Takahashi climatology. The B-SOSE and Takahashi climatology were sampled at the grid points nearest to each individual float profile. The data points for $\Delta DIC/\Delta NO_3$ in each seasonal cycle were then binned by 5° of latitude and a mean and 90% confidence interval were calculated from $\Delta DIC/\Delta NO_3$ values in each bin (Table 1). These $\Delta DIC/\Delta NO_3$ values are less sensitive to the influence of major water mass changes that result from float motion.

The observational results from both the floats and the Takahashi climatology show an increase in $\Delta DIC/\Delta NO_3$ in the low nitrate waters equatorward of 40°S (Figure 5). The B-$SOSE_{PP}$ $\Delta DIC/\Delta NO_3$ values show a more modest increase toward the equator. The $\Delta DIC/\Delta NO_3$ ratios have a direct dependence on air-sea CO_2 exchange as well as the C:N uptake ratio by phytoplankton. If we can ignore the effects of advection and mixing during the October through February period when the mixed layer is shoaling, then the change in nitrate concentration with time is (Johnson, Plant, Dunne, et al., 2017)

$$\Delta NO_3/\Delta t = -NCP/C:N + (ADV\_N + DIF\_N) \approx -NCP/C:N \quad (1)$$

where NO_3 is the salinity normalized nitrate concentration, ADV_N is the advective divergence of nitrate, DIF_N represents the diffusive nitrate concentration change, and the net community production (NCP) is a positive number for production (mol C m^{-3} d^{-1}). C:N is the ratio of carbon to nitrogen consumed by phytoplankton. The same assumptions for salinity normalized DIC give its rate of change as

Table 1
Seasonal (October Through February) Changes in DIC and Nitrate Concentration in the Upper 30 m ($\Delta DIC/\Delta NO_3$; mol C mol N^{-1}) and the Estimate Phytoplankton Uptake Ratio (C:N) Binned by Latitude From Floats, B-SOSE, and the Takahashi Climatology

	Floats		B-$SOSE_{PP}$		Takahashi	
Latitude bin	Mean $\Delta DIC/\Delta NO_3$	C:N = $\Delta DIC/\Delta NO_3$/Bias	Mean $\Delta DIC/\Delta NO_3$	Bias (Mean/6.6)	Mean $\Delta DIC/\Delta NO_3$	C:N = $\Delta DIC/\Delta NO_3$/Bias
−30	21.4 ± 5.3	10.4 ± 4.1	13.6 ± 4.1	2.06	12.1 ± 3.4	5.9 ± 2.4
−35	16.9 ± 3.9	14.0 ± 4.8	7.9 ± 2.0	1.20	17.2 ± 3.5	14.3 ± 4.6
−40	10.4 ± 1.5	9.7 ± 1.7	7.1 ± 0.7	1.07	11.8 ± 1.7	11.0 ± 1.9
−45	7.2 ± 0.5	7.1 ± 0.6	6.7 ± 0.3	1.02	7.8 ± 2.2	7.6 ± 2.2
−50	7.3 ± 0.5	6.4 ± 0.5	7.5 ± 0.3	1.14	6.4 ± 1.2	5.6 ± 1.1
−55	8.3 ± 0.7	7.6 ± 0.7	7.2 ± 0.3	1.09	4.9 ± 0.5	4.5 ± 0.5
−60	7.2 ± 1.3	7.2 ± 1.3	6.6 ± 0.3	1.00	5.8 ± 0.9	5.8 ± 1.0
−65	6.7 ± 0.8	5.6 ± 0.9	7.8 ± 0.9	1.19	8.1 ± 1.5	6.8 ± 1.5
−70	5.9 ± 0.5	4.2 ± 0.6	9.3 ± 1.1	1.41	3.1 ± 1.5	2.2 ± 1.1

Note. Error bars are 90% confidence intervals.

21699291, 2022, 9, Downloaded from https://agupubs.onlinelibrary.wiley.com/doi/10.1029/2022JC018859 by Noaa Department Of Commerce, Wiley Online Library on [21/04/2023]. See the Terms and Conditions (https://onlinelibrary.wiley.com/terms-and-conditions) on Wiley Online Library for rules of use; OA articles are governed by the applicable Creative Commons License

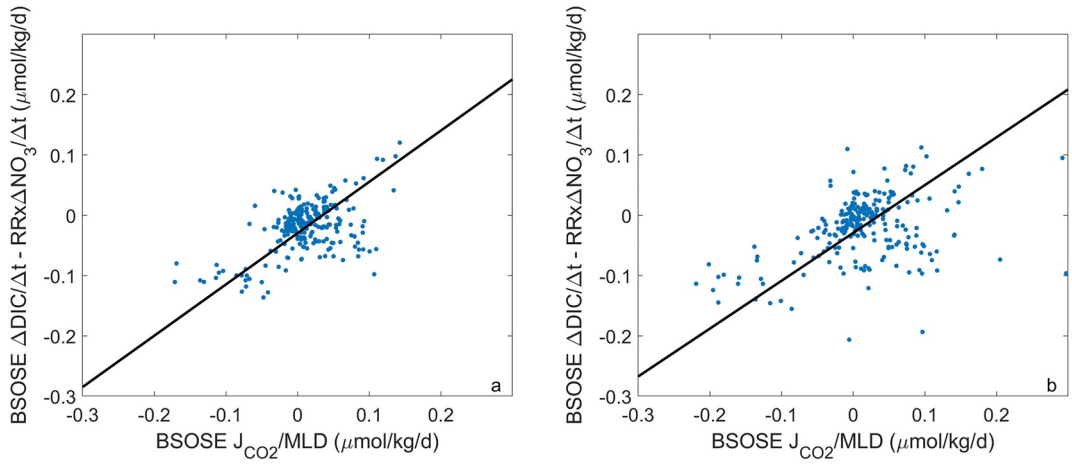

Figure 6. B-SOSE values of $\Delta DIC/\Delta t - RR \times \Delta NO_3/\Delta t$ versus J_{CO2}/MLD. (a) Values calculated using B-SOSE$_{MP}$ at the median position of each float seasonal cycle. Slope is 0.85, $R = 0.54$, 1 SD = 0.05. (b) Values calculated using B-SOSE$_{PP}$ where the model values in each seasonal cycle are at the position of each float profile. Slope is 0.79, $R = 0.38$, 1 SD = 0.05. In both panels, each point is the mean value for each of the 5 model years.

$$\Delta DIC/\Delta t = -NCP + J_{CO2}/MLD + ADV\_C + DIF\_C \approx -NCP + J_{CO2}/MLD \quad (2)$$

where J_{CO2} is the air-sea flux of carbon dioxide (mol C m^{-2} d^{-1}) with a positive value when CO_2 flux is from air to sea and ADV_C and DIF_C are the advective and diffusive DIC terms. MLD is mixed layer depth. The two equations are combined to yield

$$\Delta DIC/\Delta NO_3 = C : N\ (1 - J_{CO2}/MLD/NCP) \quad (3)$$

The effect of ignoring advection can be evaluated in B-SOSE, where C:N = RR, by taking the difference of Equation 2 minus Equation 1

$$\Delta DIC/\Delta t - RR\ x \Delta NO_3/\Delta t \approx J_{CO2}/MLD \quad (4)$$

The B-SOSE values of $\Delta DIC/\Delta t - RR \times \Delta NO_3/\Delta t$ are plotted versus J_{CO2}/MLD in Figure 6a with B-SOSE$_{MP}$ data and Figure 6b for B-SOSE$_{PP}$ using each of the 243 time series. Each data point is the mean value for the October to February period in 5 model years. J_{CO2} was computed as the mean of monthly mean values in each seasonal series. MLD was taken as the maximum value in each month because the change in DIC from gas exchange reflects the deepest mixing event, not the mean. The slopes of regression lines through the data in both Figures 6a and 6b are near 0.8. These comparisons represent the signal seen by floats, and not the Lagrangian change that occurs in water parcels, which would be the proper assessment of Equation 4. The Lagrangian assessment is beyond the scope of this study. The agreement of the slopes from the two approaches suggests that Equation 4 captures the major processes that dominate the variability of $\Delta DIC/\Delta t$ relative to the value expected from $\Delta NO_3/\Delta t$. Advection and mixing clearly affect individual data points, creating the scatter about the regression line and the shift in slope from the expected value of 1. In the case of B-SOSE$_{PP}$, this variability is even greater than in B-SOSE$_{MP}$ (Figure 6). However, the overall trend of the data is close to the expected slope of 1. The effects of the mixing and transport mechanisms mostly cancel out when the array as a whole is considered in Equation 4.

Similar logic applies to Equation 3. Individual data points will be biased by advection and mixing, but for groups of floats, air-sea flux will shift $\Delta DIC/\Delta NO_3$ in a well-defined manner. Equation 3 predicts that $\Delta DIC/\Delta NO_3$ is greater than the biological C to N uptake ratio (C:N) if J_{CO2} is negative, which corresponds to a flux out of the ocean. This results because NCP is positive during the bloom months considered here. Following from Equation 3, the $\Delta DIC/\Delta NO_3$ increase toward the equator in B-SOSE$_{PP}$ is due primarily to a negative J_{CO2} equatorward of 40°S in the October to February time period that results from seasonal warming and outgassing of CO_2.

The B-SOSE$_{PP}$ trend equatorward of 40°S represents the effects of J_{CO2} on the value of ΔDIC and any residual effects of mixing and advection on DIC and nitrate. The larger trend in float $\Delta DIC/\Delta NO_3$ to the north of

21699291, 2022, 9, Downloaded from https://agupubs.onlinelibrary.wiley.com/doi/10.1029/2022JC018859 by Noaa Department Of Commerce, Wiley Online Library on [21/04/2023]. See the Terms and Conditions (https://onlinelibrary.wiley.com/terms-and-conditions) on Wiley Online Library for rules of use; OA articles are governed by the applicable Creative Commons License

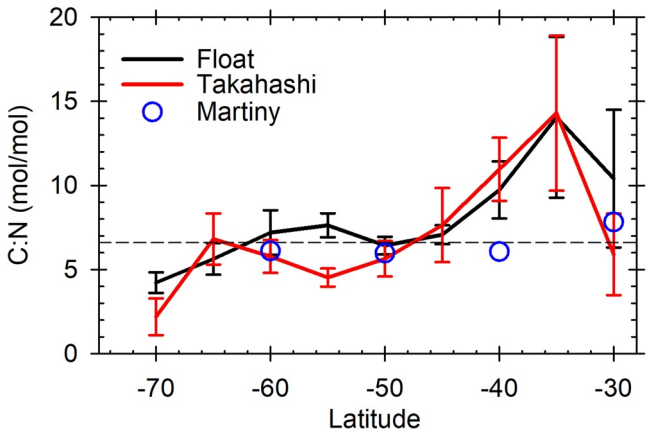

Figure 7. Mean and 90% confidence intervals of the 5° binned C:N values that were obtained after correcting the float (black) and Takahashi (red) $\Delta DIC/\Delta NO_3$ values by the bias factor found in B-$SOSE_{PP}$ (Table 1). Mean C:N values derived from the binned (by 10°) values of C:P and C:N reported by Martiny, Pham, et al. (2013) are shown as blue circles. The horizontal dashed line is at C:N = 6.6.

40°S, relative to B-$SOSE_{PP}$, must then be due to an increasing C:N value. We use the ratio of the B-$SOSE_{PP}$ $\Delta DIC/\Delta NO_3$ values in each bin, relative to RR, to estimate the bias factor due to processes other than biological uptake (Table 1). The bias factor ranges from 1.0 to 2.0.

The float and Takahashi $\Delta DIC/\Delta NO_3$ values were then corrected by the bias factor found in the B-SOSE model to estimate the biological C:N ratio in each bin (Table 1). These corrected float C:N values increase to near 15 in the bins equatorward of 40°S (Figure 7), where nitrate becomes a limiting nutrient. A similar trend in $\Delta DIC/\Delta NO_3$ was found along a transect from 30°N to 60°N in the North Atlantic by comparing concentrations measured in summer with estimated winter values (Körtzinger, Koeve, et al., 2001). A large increase in $\Delta DIC/\Delta NO_3$ occurred in subtropical waters.

The exact $\Delta DIC/\Delta NO_3$ or C:N values in each bin of the float data equatorward of 40°S are somewhat subjective because of large uncertainty in the ΔNO_3 term. As ΔNO_3 goes to 0, even its sign becomes uncertain in both the float data and Takahashi climatology and its presence as a denominator magnifies uncertainty in $\Delta DIC/\Delta NO_3$ (Figure 2d). If the ratios were calculated as ΔNO_3:ΔDIC, they would be near 0. To control for this effect, the binned $\Delta DIC/\Delta NO_3$ values were calculated using only seasonal cycles where $|\Delta NO_3| > 0.5$ μmol/kg over the seasonal cycle. This removed 17 of 34 cycles. Elimination of these cycles, which have the highest $\Delta DIC/\Delta NO_3$ values due to very low ΔNO_3, reduces the mean of the binned values. The mean float and Takahashi $\Delta DIC/\Delta NO_3$ values in Figure 5 and Table 1 are minimum estimates, therefore.

These large seasonal drawdowns in DIC without a corresponding change in nitrate are consistent with observations at the Bermuda Atlantic Time-series Station (BATS), which is another low nutrient environment. Large seasonal declines in DIC due to NCP occur while the corresponding nitrate concentration changes are much less than would be required by the RR (Karl et al., 2003; Michaels et al., 1994). As noted by Fawcett et al. (2018), the very high C:N ratio is hypothesized to result from the production of a gel-like organic matter that is extremely depleted in nitrogen, relative to the amount of carbon. This material does not accumulate on filters and appears as dissolved organic carbon (DOC), although it may aggregate and sink with mineral ballast. Hansell and Carlson (1988) found that 60%–70% of NCP in the Sargasso Sea may appear as DOC. A large accumulation of DOC is found in the oligotrophic southeast Pacific equatorward of 40°S, but not dissolved organic nitrogen (Bif et al., 2022). This is supportive of the hypothesis proposed by Fawcett et al. (2018). Similar large DOC increases are seen in all subtropical ocean basins (Hansell et al., 2009).

The apparent high C:N uptake ratios could also stem from elevated carbon uptake by nutrient-stressed phytoplankton, as seen in laboratory experiments (Geider et al., 1998; Laws & Bannister, 1980). Phytoplankton biomass in oligotrophic environments, typical of the ocean north of 40°S, are often dominated by photosynthetic bacteria such as *Prochlorococcus*. Lomas et al. (2021) have shown that oceanic *Prochlorococcus* populations may have C:N ratios >10 when nitrogen stressed due to continued accumulation of cellular carbon through photosynthesis. However, they also note that it is not clear that this accumulation of carbon is retained. Laboratory experiments show that *Prochlorococcus* may retain little of the carbon they fix when nutrient stressed (Szul et al., 2019).

Such behavior by nutrient-stressed phytoplankton would be consistent with the model proposed by Fawcett et al. (2018). Following this model (Fawcett et al., 2018), phytoplankton continue to produce organic carbon as DOC in oligotrophic systems that are deficient in inorganic nitrogen. This extracellular release of DOC by nutrient-starved phytoplankton is termed the overflow model (Carlson & Hansell, 2015 and references therein). It serves as an adaptive strategy by phytoplankton to protect the cell from photochemical damage and it allows the cell to maintain its photochemical machinery, particularly in times of nutrient stress. The exuded material would accumulate in surface waters because heterotrophic bacteria lack the nutrients needed to grow on it. A drawdown in DIC and an accumulation of oxygen will then occur with little accumulation of phytoplankton biomass. A gel-like nature that allowed the DOC to aggregate inorganic ballast and then to be removed by very slow settling, or through diffusion or convective overturn, would eventually transport it to the nutricline. At that

21699291, 2022, 9, Downloaded from https://agupubs.onlinelibrary.wiley.com/doi/10.1029/2022JC018859 by Noaa Department Of Commerce, Wiley Online Library on [21/04/2023]. See the Terms and Conditions (https://onlinelibrary.wiley.com/terms-and-conditions) on Wiley Online Library for rules of use; OA articles are governed by the applicable Creative Commons License

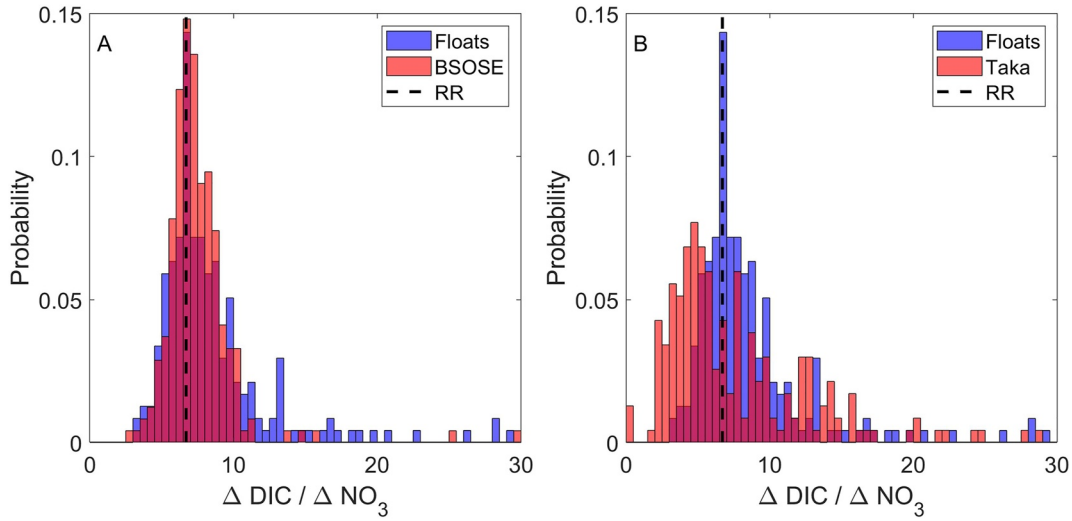

Figure 8. Histograms of the $\Delta DIC/\Delta NO_3$ values found in the 243 seasonal drawdown cycles for (a) floats (blue) and B-SOSE (red), and (b) for the float (blue) and Takahashi (red) data sets.

point, nitrate assimilating, heterotrophic bacteria could metabolize the material. Particulate matter in these environments would retain a C:N ratio consistent with Redfield, as observed in the Pacific Sector of the Southern Ocean (Lee et al., 2021). Export of this particulate matter to the deep ocean would produce a Redfield signal in deep, dissolved oxygen, carbon, and nitrate. Thus, two cycles may be operating in these waters as hypothesized by Fawcett et al. (2018): a particulate cycle at Redfield proportions and a non-Redfield cycle with high C:N in near-surface waters.

Such a process would account for the anomalously high oxygen production (Emerson, 2014) and DIC uptake rates (Keeling et al., 2004; Michaels et al., 1994) that characterize the euphotic zone of oligotrophic oceans, as well as the non-Redfield remineralization ratios seen seasonally in the nutricline where the nitrogen poor, gel-like material is consumed (Fawcett et al., 2018). The relatively high DIC depletion rate, and corresponding O_2 production rate in the euphotic zone, would be interpreted as high NCP. These high NCP rates derived from DIC depletion would explain the observation by Emerson (2014) of relatively little variation in annual NCP determined by geochemical mass balance across the global ocean. Rapid metabolism of the organic material and slow sinking rates would prevent export below the nutricline. This would allow the ratios of $\Delta DIC/\Delta NO_3$ determined from changes in chemistry beneath the seasonal pycnocline to remain similar to RR except within the nutricline where the gel-like organic matter was metabolized, as observed by Fawcett et al. (2018).

The binned $\Delta DIC/\Delta NO_3$ values from 45°S to 65°S in the float data are slightly larger than the Redfield value (Figure 5, Table 1). The B-$SOSE_{PP}$ $\Delta DIC/\Delta NO_3$ values in the 45°S to 65°S latitude range also tend to be larger than the RR value that is inherent to biological processes in the model. The difference between the B-$SOSE_{PP}$ $\Delta DIC/\Delta NO_3$ values and RR implies that air-sea gas exchange has increased the ΔDIC term. The binned float values of C:N that were corrected using the bias seen in B-$SOSE_{PP}$ range from 6.4 ± 0.5 (90% CI) to 7.6 ± 0.7 from 45°S to 60°S (Table 1). With the exception of the binned data at 55°S, the derived C:N values are not significantly different from RR (Figure 7).

Similar calculations were performed on the Takahashi climatology. The corrected Takahashi C:N values range from 4.3 ± 0.6 to 7.7 ± 2.2 (Figure 7, Table 1). The corrected Takahashi value at 55°S is significantly lower than RR, in contrast to the value based on float data.

4.3. Implications of $\Delta DIC/\Delta NO_3$ for J_{CO2}

Histograms of the $\Delta DIC/\Delta NO_3$ values for floats, B-SOSE, and the Takahashi data sets are shown in Figure 8. There was no statistical difference between the float and B-$SOSE_{PP}$ values (*t*-test, $p = 0.8$). The histogram of the values derived from the Takahashi climatology is shifted lower than the float data (Figure 8b). The mean of the $\Delta DIC/\Delta NO_3$ values for each seasonal cycle extracted from the Takahashi climatology (5.99) was below the

21699291, 2022, 9, Downloaded from https://agupubs.onlinelibrary.wiley.com/doi/10.1029/2022JC018859 by Noaa Department Of Commerce, Wiley Online Library on [21/04/2023]. See the Terms and Conditions (https://onlinelibrary.wiley.com/terms-and-conditions) on Wiley Online Library for rules of use; OA articles are governed by the applicable Creative Commons License

21699291, 2022, 9, Downloaded from https://agupubs.onlinelibrary.wiley.com/doi/10.1029/2022JC018859 by Noaa Department Of Commerce, Wiley Online Library on [21/04/2023]. See the Terms and Conditions (https://onlinelibrary.wiley.com/terms-and-conditions) on Wiley Online Library for rules of use; OA articles are governed by the applicable Creative Commons License

Redfield value and significantly lower ($p < 0.001$ in either a *t*-test or a Kruskal-Wallis nonparametric Analysis of Variance on Ranks) than the mean of both the corresponding float (7.35) and B-SOSE (7.27) data sets. Much of this difference arises from the large number of values around 55°S, where the Takahashi data set has many values that lie below the line that delimits the RR (Figure 5b). There is also a difference in the float and Takahashi $\Delta DIC/\Delta NO_3$ values in the 30°S bin that is just significant. In the following, we focus on a possible cause of the difference at 55°S, and not at 30°S. Much of the difference at 30°S arises from the nitrate data, which is near 0 and small changes in the denominator of $\Delta DIC/\Delta NO_3$ have a large effect. Large changes in DIC with small values of ΔNO_3 constrain $\Delta DIC/\Delta NO_3$ to be large in both data sets, but the significance of the difference is uncertain.

The difference in float and Takahashi $\Delta DIC/\Delta NO_3$ near 55°S may be related to a temporal change. The pCO_2 data used to construct the Takahashi climatology were referenced to the year 2005. To accomplish this, the measured pCO_2 values were adjusted to the value they would have had in the year 2005 by assuming they were changing in time at the same rate that CO_2 was accumulating in the atmosphere. The derived DIC concentrations in the Takahashi climatology thus represent an estimate of the values that would have been found in 2005. The profiling float data were all obtained from 2014 through 2021, with an average date of January 2019. Presuming no large biases in either set of observations, there are three explanations for the difference in the $\Delta DIC/\Delta NO_3$ in the float data and the Takahashi climatology around 55°S. First, the ratio of phytoplankton uptake of carbon and nitrogen could have been much lower than RR around the Takahashi reference year of 2005 and above RR in the time frame of the float data. Second, discrepancies in spatial or seasonal sampling of the Takahashi data could bias the comparison. Or third, following Equation 3, the ocean sampled during October through February at the float profile locations in the 55°S band could have shifted from a CO_2 sink ($J_{CO2}>0$) in the Takahashi climatology reference year of 2005 to a source ($J_{CO2}<0$) during the years sampled by the floats.

The C:N ratios for phytoplankton uptake that are obtained from both the float data or the Takahashi climatology south of 40°S are relatively consistent with observations of particulate matter composition in the Southern Ocean. Martiny, Pham, et al. (2013) and Martiny, Vrugt, et al. (2013) report a global set of carbon, nitrogen, and phosphorous measurements in marine organic particles. The C:N values derived from the mean N:P and C:P data binned by latitude in supplementary table S3 of Martiny, Pham, et al. (2013) are compared with the binned C:N values from floats and the Takahashi climatology (Figure 7). There is little difference from the RR for particle composition in most bins to the south of 40°S. It seems unlikely that the difference in C:N at 55°S represents a change in C:N of phytoplankton uptake.

Much of the Takahashi climatology in the Southern Ocean is based on values interpolated from a sparse set of observations. This is particularly true for observations in winter months. It is essentially impossible to control for the lack of underlying observations in the gridded data compiled by Takahashi et al. (2014). In contrast, each of the float time series is built on a set of direct observations of pH and nitrate and the values do not involve extrapolation in space or time. They do require a conversion of pH to DIC, which has little uncertainty (Figure 1 and Williams et al., 2017). The long extrapolations needed to build the Takahashi climatology may account for the difference in C:N at 55°S, but it is remarkable that the C:N values match so closely with the float and Martiny, Pham, et al. (2013) results elsewhere in the region south of 40°S.

The consistency of the $\Delta DIC/\Delta NO_3$ values in the float and Takahashi climatology in most of the zonal bands south of 40°S (Figure 5) suggests that the flux of CO_2 due to air-sea exchange from October through February was similar in the reference year 2005 of the Takahashi climatology and the 2014–2021 float period. While Southern Ocean CO_2 fluxes have oscillated in time with positive and negative trends (Landschützer et al., 2015), the overall trend of flux has been toward increasing uptake into the ocean at a rate corresponding to 0.009 mol C m^{-2} y^{-1}. Equation 3 implies that this would have decreased $\Delta DIC/\Delta NO_3$ from 6.6 in the absence of air-sea exchange 6.6 to 6.4 over one decade at a mean integrated NCP rate of 2 mol C m^{-2} y^{-1} (Johnson, Plant, Dunne, et al., 2017). This change would not be detectable with the uncertainty of the binned data in most of the latitude bands south of 30°S (Table 1). However, the $\Delta DIC/\Delta NO_3$ values for floats and Takahashi are statistically different in the 55°S band (Table 1). The difference corresponds to a change in the air-sea flux during October to February of 2005 and the float period at a rate equivalent 1.5 mol C m^{-2} y^{-1} with the flux moving from ingassing in 2005 toward outgassing.

Given the consistency of the float and Takahashi C:N values with the RR across the other regions from 45°S to 65°S, one would expect C:N to also be consistent with the RR at 55°S. If that is so, then Equation 3 would imply

21699291, 2022, 9, Downloaded from https://agupubs.onlinelibrary.wiley.com/doi/10.1029/2022JC018859 by Noaa Department Of Commerce, Wiley Online Library on [21/04/2023]. See the Terms and Conditions (https://onlinelibrary.wiley.com/terms-and-conditions) on Wiley Online Library for rules of use; OA articles are governed by the applicable Creative Commons License

that the 55°S band was losing CO_2 to the atmosphere from October through February in the float years, giving a C:N value that was higher than RR. During the reference period of the Takahashi climatology, the C:N value lower than RR implies that the ocean was gaining CO_2 from the atmosphere. An ocean CO_2 uptake flux of about 0.7 mol C m^{-2} y^{-1} in the October to February time frame of the Takahashi data set (Landschützer et al., 2020) would then suggest that the 55°S band is now outgassing at about 0.7 mol C m^{-2} y^{-1} if C:N were at the Redfield value. Such a difference from circa 2005 to the float period of 2014–2021 would not be consistent with the gridded compilation of global CO_2 fluxes produced by fitting shipboard data in a neural network (Landschützer et al., 2016). The neural network product (Landschützer et al., 2020) finds the ocean from 50°S to 60°S to be taking up more CO_2 in the 5 months beginning October of the years from 2014 to 2020 when compared to the same period in 2005. However, air-sea CO_2 fluxes derived from profiling float pH values are more negative (outgassing) than the Landschützer product in the Antarctic-Southern Zone, which corresponds closely to the 55°S band (Bushinsky et al., 2019; Gray et al., 2018). The difference has been attributed to sparse sampling in space and time of the ship-based product rather than a systematic bias in flux (Bushinsky et al., 2019). The change in flux reported by Gray et al. (2018), relative to the ship-based products in the Antarctic-Southern Zone, is of the correct magnitude and direction to account for the difference of $\Delta DIC/\Delta NO_3$ in the float and Takahashi data sets. However, there are also suggestions of a systematic bias in the float data (Long et al., 2021). A relatively small, systematic offset (~0.005) in the quality controlled float pH data used to compute pCO_2 and CO_2 flux could account for much of the difference in the Antarctic-Southern Zone. This bias would only be present in pH data from the Antarctic-Southern Zone as fluxes generated from float pH values were much more consistent with the ship-based CO_2 fluxes in other areas (Gray et al., 2018).

5. Conclusions

The seasonal drawdowns in DIC and nitrate in 243 seasonal cycles across the Southern Ocean are highly correlated across all cycles. Within each cycle, the concentrations of DIC and nitrate are also generally correlated and can be used to provide an estimate of the carbon to nitrate ratio taken up by phytoplankton. After correcting for gas exchange and mixing and advection effects using the B-SOSE model, we find values of C:N larger than the RR to the north of 40°S. This is the most oligotrophic region with little nitrate in surface waters. The large C:N values north of 40°S are consistent with observations of large $\Delta DIC/\Delta t$ and small $\Delta NO_3/\Delta t$ in other oligotrophic regions (Karl et al., 2003; Michaels et al., 1994). Much larger amounts of DIC are consumed by phytoplankton than might be expected from nitrate availability and this is very likely due to the hypothesized production of a gel-like organic matter that is depleted in nitrogen (Fawcett et al., 2018). This process would produce estimates of NCP based on oxygen or DIC that are much larger than expected from net primary production. It would account for observations of "carbon overconsumption" as nutrients are depleted (Körtzinger, Hedges, et al., 2001; Sambrotto et al., 1993; Toggweiler, 1993). In the latitudes from 40°S to 65°S, C:N uptake generally occurs at a ratio close to the expected RR.

The $\Delta DIC/\Delta NO_3$ data also suggest a shift from an ocean sink for atmospheric CO_2 in the Takahashi reference year of 2005 near 55°S to an ocean CO_2 source during the months of October through February in the float years. This region corresponds closely to the Antarctic-Southern Zone (Gray et al., 2018). It appears as an area of significant outgassing in the analysis of J_{CO2} values derived from profiling float observations (Bushinsky et al., 2019; Gray et al., 2018). The outgassing derived from analyses using float data exceeds the values based on the mostly ship-based data set (Bushinsky et al., 2019; Landschützer et al., 2015). Thus, assessments based on the seasonal change in surface DIC stocks (this work), or annual mean air-sea CO_2 fluxes (Bushinsky et al., 2019; Gray et al., 2018) could indicate a recent change in the ocean air-sea carbon flux in the Antarctic-Southern Zone. Alternative explanations involving bias in pCO_2 estimates (Long et al., 2021) or sampling (Bushinsky et al., 2019) could also account for the difference in flux, but these explanations would not account for the apparent change in $\Delta DIC/\Delta NO_3$ we compute at 55°S relative to the value derived from the Takahashi climatology. Observed ocean and atmospheric changes such as deepening mixed layers (Sallée et al., 2021), warming (Gille, 2008; Roemmich et al., 2015), freshening (Swart et al., 2018), increasing currents (Shi et al., 2021), and strengthening winds (Swart and Fyfe, 2012; Toggweiler and Russell, 2008) may be associated with a shift in CO_2 gas flux.

Data Availability Statement

All data used in this study are available online at the sources listed in Sections 2 and 3.

Acknowledgments
Profiling float data were collected and made freely available by the Southern Ocean Carbon and Climate Observations and Modeling (SOCCOM) Project funded by the National Science Foundation, Division of Polar Programs (NSF PLR-1425989 and OPP-1936222), supplemented by NOAA Grant NA20OAR4320271, NASA Grant NNX14AP49G, and by the International Argo Program and the national programs that contribute to it (http://www.argo.ucsd.edu, http://argo.jcommops.org). The Argo Program is part of the Global Ocean Observing System. The B-SOSE model development was also supported through the SOCCOM project. Work at MBARI is also supported by the David and Lucile Packard Foundation. The authors thank all of the personnel who have contributed to the construction of the profiling float array, personnel who have assisted at sea in deployments, and the captains and crew of the vessels that have deployed these floats. The authors particularly thank Prof. Jorge Sarmiento for his skill in directing SOCCOM and Dr. Roberta Hotinski for her wise management of the program.

References

Anderson, L. A., & Sarmiento, J. L. (1994). Redfield ratios of remineralization determined by nutrient data analysis. *Global Biogeochemical Cycles*, *8*(1), 65–80. https://doi.org/10.1029/93GB03318

Arrigo, K. R., Robinson, D. H., Worthen, D. L., Dunbar, R. B., DiTullio, G. R., VanWoert, M., & Lizotte, M. P. (1999). Phytoplankton community structure and the drawdown of nutrients and CO_2 in the Southern Ocean. *Science*, *283*(5400), 365–367. https://doi.org/10.1126/science.283.5400.365

Arroyo, M. C., Shadwick, E. H., Tilbrook, B., Rintoul, S. R., & Kusahara, K. (2020). A continental shelf pump for CO_2 on the Adélie Land coast, East Antarctica. *Journal of Geophysical Research: Oceans*, *125*, e2020JC016302. https://doi.org/10.1029/2020JC016302

Balch, W. M., Bates, N. R., Lam, P. J., Twining, B. S., Rosengard, S. Z., Bowler, B. C., et al. (2016). Factors regulating the Great Calcite Belt in the Southern Ocean and its biogeochemical significance. *Global Biogeochemical Cycles*, *30*, 1124–1144. https://doi.org/10.1002/2016GB005414

Bif, M. B., Bourbonnais, A., Hansell, D. A., Granger, J., Westbrook, H., & Altabet, M. A. (2022). Controls on surface distributions of dissolved organic carbon and nitrogen in the upper southeast Pacific Ocean. *Marine Chemistry*, *244*, 104136. https://doi.org/10.1016/j.marchem.2022.104136

Bittig, H. C., Steinhoff, T., Claustre, H., Fiedler, B., Williams, N. L., Sauzède, R., et al. (2018). An alternative to static climatologies: Robust estimation of open ocean CO_2 variables and nutrient concentrations from T, S, and O_2 data using Bayesian neural networks. *Frontiers in Marine Science*, *5*, 328. https://doi.org/10.3389/fmars.2018.00328

Brix, H., Currie, K. I., & Fletcher, S. E. M. (2013). Seasonal variability of the carbon cycle in subantarctic surface water in the South West Pacific. *Global Biogeochemical Cycles*, *27*, 200–211. https://doi.org/10.1002/gbc.20023

Bushinsky, S. M., Landschützer, P., Rödenbeck, C., Gray, A. R., Baker, D., Mazloff, M. R., et al. (2019). Reassessing Southern Ocean air-sea CO_2 flux estimates with the addition of biogeochemical float observations. *Global Biogeochemical Cycles*, *33*, 1370–1388. https://doi.org/10.1029/2019GB006176

Carlson, C. A., & Hansell, D. A. (2015). DOM sources, sinks, reactivity, and budgets. In D. A. Hansell, & C. A. Carlson (Eds.), *Biogeochemistry of marine dissolved organic matter* (2nd ed., pp. 65–126). Amsterdam: Elsevier Inc. https://doi.org/10.1016/B978-0-12-405940-5.00003-0

Carter, B. R., Feely, R. A., Williams, N. L., Dickson, A. G., Fong, M. B., & Takeshita, Y. (2018). Updated methods for global locally interpolated estimation of alkalinity, pH, and nitrate. *Limnology and Oceanography: Methods*, *16*, 119–131. https://doi.org/10.1002/lom3.10232

Conkright, M., Levitus, S., & Boyer, T. (1994). *World Ocean Atlas 1994: Nutrients* (Vol. 1). Silver Spring, MD: National Oceanic and Atmospheric Administration.

Copin-Montegut, C., & Copin-Montegut, G. (1983). Stoichiometry of carbon, nitrogen, and phosphorus in marine particulate matter. *Deep-Sea Research Part I*, *30*, 31–46. https://doi.org/10.1016/0198-0149(83)90031-6

Deutsch, C., & Weber, T. (2012). Nutrient ratios as a tracer and driver of ocean biogeochemistry. *Annual Reviews of Marine Science*, *4*, 113–141. https://doi.org/10.1146/annurev-marine-120709-142821

DeVries, T. (2018). New directions for ocean nutrients. *Nature Geoscience*, *11*(1), 15–16. https://doi.org/10.1038/s41561-017-0042-z

Emerson, S. (2014). Annual net community production and the biological carbon flux in the ocean. *Global Biogeochemical Cycles*, *28*, 14–28. https://doi.org/10.1002/2013GB004680

Fawcett, S. E., Johnson, K. S., Riser, S. C., Oostende, V., & Sigman, D. M. (2018). Low-nutrient organic matter in the Sargasso Sea thermocline: A hypothesis for its role, identity, and carbon cycle implications. *Marine Chemistry*, *207*, 108–123. https://doi.org/10.1016/j.marchem.2018.10.008

Galbraith, E. D., Gnanadesikan, A., Dunne, J. P., & Hiscock, M. R. (2010). Regional impacts of iron-light colimitation in a global biogeochemical model. *Biogeosciences*, *7*, 1043–1064. https://doi.org/10.5194/bg-7-1043-2010

Geider, R. J., MacIntyre, H. J., & Kana, T. M. (1998). A dynamic regulatory model of phytoplankton acclimation to light, nutrients and temperature. *Limnology & Oceanography*, *43*, 679–694. https://doi.org/10.4319/lo.1998.43.4.0679

Gille, S. T. (2008). Decadal-scale temperature trends in the Southern Hemisphere Ocean. *Journal of Climate*, *21*, 4749–4765. https://doi.org/10.1175/2008jcli2131.1

Gray, A. R., Johnson, K. S., Bushinsky, S. M., Riser, S. C., Russell, J. L., Talley, L. D., et al. (2018). Autonomous biogeochemical floats detect significant carbon dioxide outgassing in the high-latitude Southern Ocean. *Geophysical Research Letters*, *45*(17), 9049–9057. https://doi.org/10.1029/2018GL078013

Hansell, D. A., & Carlson, C. A. (1998). Net community production of dissolved organic carbon. *Global Biogeochemical Cycles*, *12*, 443–453. https://doi.org/10.1029/98gb01928

Hansell, D. A., Carlson, C. A., Repeta, D. J., & Schlitzer, R. (2009). Dissolved organic matter in the ocean: New insights stimulated by a controversy. *Oceanography*, *22*, 52–61. https://doi.org/10.5670/oceanog.2009.109

Ishii, M., Inoue, H. Y., & Matsueda, H. (2002). Net community production in the marginal ice zone and its importance for the variability of the oceanic pCO_2 in the Southern Ocean south of Australia. *Deep Sea Research, Part II*, *49*(9–10), 1691–1706. https://doi.org/10.1016/s0967-0645(02)00007-3

Johnson, K. S. (2010). Simultaneous measurements of nitrate, oxygen, and carbon dioxide on oceanographic moorings: Observing the Redfield ratio in real time. *Limnology & Oceanography*, *55*, 615–627. https://doi.org/10.4319/lo.2010.55.2.0615

Johnson, K. S., Coletti, L., Jannasch, H., Sakamoto, C., Swift, D., & Riser, S. (2013). Long-term nitrate measurements in the ocean using the in situ ultraviolet spectrophotometer: Sensor integration into the Apex profiling float. *Journal of Atmospheric and Oceanic Technology*, *30*(8), 1854–1866. https://doi.org/10.1175/JTECH-D-12-00221.1

Johnson, K. S., Jannasch, H. W., Coletti, L. J., Elrod, V. A., Martz, T. R., Takeshita, Y., et al. (2016). Deep-Sea DuraFET: A pressure tolerant pH sensor designed for global sensor networks. *Analytical Chemistry*, *88*, 3249–3256. https://doi.org/10.1021/acs.analchem.5b04653

Johnson, K. S., Plant, J. N., Coletti, L. J., Jannasch, H. W., Sakamoto, C. M., Riser, S. C., et al. (2017). Biogeochemical sensor performance in the SOCCOM profiling float array. *Journal of Geophysical Research: Oceans*, *122*, 6416–6436. https://doi.org/10.1002/2017JC012838

Johnson, K. S., Plant, J. N., Dunne, J. P., Talley, L. D., & Sarmiento, J. L. (2017). Annual nitrate drawdown observed by SOCCOM profiling floats and the relationship to annual net community production. *Journal of Geophysical Research: Oceans*, *122*, 6668–6683. https://doi.org/10.1002/2017JC012839

21699291, 2022, 9, Downloaded from https://agupubs.onlinelibrary.wiley.com/doi/10.1029/2022JC018859 by Noaa Department Of Commerce, Wiley Online Library on [21/04/2023]. See the Terms and Conditions (https://onlinelibrary.wiley.com/terms-and-conditions) on Wiley Online Library for rules of use; OA articles are governed by the applicable Creative Commons License

Karl, D. M., Bates, N. R., Emerson, S., Harrison, P. J., Jeandel, C., Llinâs, O., et al. (2003). Temporal studies of biogeochemical processes in the world's oceans during the JGOFS era. In M. J. R. Fasham (Ed.), *Ocean biogeochemistry: The role of the ocean carbon cycle in global change* (pp. 239–267). New York: Springer. https://doi.org/10.1007/978-3-642-55844-3_11

Keeling, C. D., Brix, H., & Gruber, N. (2004). Seasonal and long-term dynamics of the upper ocean carbon cycle at station ALOHA near Hawaii. *Global Biogeochemical Cycles*, *18*, GB4006. https://doi.org/10.1029/2004GB002227

Körtzinger, A., Hedges, J. I., & Quay, P. D. (2001). Redfield ratios revisited: Removing the biasing effect of anthropogenic CO_2. *Limnology & Oceanography*, *46*(4), 964–970.

Körtzinger, A., Koeve, W., Kähler, W., & Mintrop, L. J. (2001). C: N ratios in the mixed layer during the productive season in the northeast Atlantic Ocean. *Deep-Sea Research Part I*, *48*, 661–688. https://doi.org/10.1016/S0967-0637(00)00051-0

Körtzinger, A., Send, U., Lampitt, R. S., Hartman, S., Wallace, D. W. R., Karstensen, J., et al. (2008). The seasonal pCO_2 cycle at 49°N/16.5°W in the northeastern Atlantic Ocean and what it tells us about biological productivity. *Journal of Geophysical Research*, *113*, C04020. https://doi.org/10.1029/2007JC004347

Landschützer, P., Gruber, N., & Bakker, D. C. E. (2016). Decadal variations and trends of the global ocean carbon sink. *Global Biogeochemical Cycles*, *30*, 1396–1417. https://doi.org/10.1002/2015GB005359

Landschützer, P., Gruber, N., & Bakker, D. C. E. (2020). *An observation-based global monthly gridded sea surface pCO_2 and air-sea CO_2 flux product from 1982 onward and its monthly climatology (NCEI Accession 0160558). Version 6.6*. NOAA National Centers for Environmental Information. https://doi.org/10.7289/V5Z899N6

Landschützer, P., Gruber, N., Haumann, F. A., Rödenbeck, C., Bakker, D. C. E., van Heuven, S., et al. (2015). The reinvigoration of the Southern Ocean carbon sink. *Science*, *349*(6253), 1221–1224. https://doi.org/10.1126/science.aab2620

Laws, E. A. (1997). *Mathematical methods for oceanographers: An introduction*. New York: Wiley-Interscience.

Laws, E. A., & Bannister, T. T. (1980). Nutrient- and light-limited growth of *Thalassiosira fluviatilis* in continuous culture, with implications for phytoplankton growth in the ocean. *Limnology & Oceanography*, *25*, 457–473. https://doi.org/10.4319/lo.1980.25.3.0457

Lee, J. A., Garcia, C. A., Larkin, A. A., Carter, B. R., & Martiny, A. C. (2021). Linking a latitudinal gradient in ocean hydrography and elemental stoichiometry in the eastern Pacific Ocean. *Global Biogeochemical Cycles*, *35*, e2020GB006622. https://doi.org/10.1029/2020GB006622

Lewis, E., & Wallace, D. W. R. (1998). *CO2SYS-Program developed for the CO2 system calculations ORNL/CDIAC-105*. Carbon Dioxide Information Analysis Center, Oak Ridge National Laboratory, US DoE.

Lomas, M. W., Baer, S. E., Mouginot, C., Terpis, K. X., Lomas, D. A., Altabet, M. A., & Martiny, A. C. (2021). Varying influence of phytoplankton biodiversity and stoichiometric plasticity on bulk particulate stoichiometry across ocean basins. *Communications Earth & Environment*, *2*(1), 1–10. https://doi.org/10.1038/s43247-021-00212-9

Long, M. C., Stephens, B. B., McKain, K., Sweeney, C., Keeling, R. F., Kort, E. A., et al. (2021). Strong Southern Ocean carbon uptake evident in airborne observations. *Science*, *374*(6572), 1275–1280. https://doi.org/10.1126/science.abi4355

Louanchi, F., Ruiz-Pino, D. P., Jeandel, C., Brunet, C., Schauer, B., Masson, A., et al. (2001). Dissolved inorganic carbon, alkalinity, nutrient and oxygen seasonal and interannual variations in the upper ice-free Antarctic ocean. *Deep Sea Research Part I*, *48*, 1581–1603. https://doi.org/10.1016/s0967-0637(00)00086-8

Martiny, A. C., Pham, C. T. A., Primeau, F. W., Vrugt, J. A., Moore, J. K., Levin, S. A., & Lomas, M. W. (2013). Strong latitudinal patterns in the elemental ratios of marine plankton and organic matter. *Nature Geoscience*, *6*, 279–283. https://doi.org/10.1038/ngeo1757

Martiny, A. C., Vrugt, J. A., Primeau, F. W., & Lomas, M. W. (2013). Regional variation in the particulate organic carbon to nitrogen ratio in the surface ocean. *Global Biogeochemical Cycles*, *27*, 723–731. https://doi.org/10.1002/gbc.20061

Martz, T., Send, U., Ohman, M. D., Takeshita, Y., Bresnahan, P., Kim, H.-J., & Nam, S. H. (2014). Dynamic variability of biogeochemical ratios in the Southern California Current System. *Geophysical Research Letters*, *41*, 2496–2501. https://doi.org/10.1002/2014GL059332

Maurer, T. L., Plant, J. N., & Johnson, K. S. (2021). Delayed-mode quality control of oxygen, nitrate, and pH data on SOCCOM biogeochemical profiling floats. *Frontiers in Marine Science*, *8*, 683207. https://doi.org/10.3389/fmars.2021.683207

Michaels, A. F., Bates, N. R., Buesseler, K. O., Carlson, C. A., & Knap, A. H. (1994). Carbon-cycle imbalances in the Sargasso Sea. *Nature*, *372*(6506), 537–540. https://doi.org/10.1038/372537a0

Orsi, A. H., Whitworth, T., III, & Nowlin, W. D., Jr. (1995). On the meridional extent and fronts of the Antarctic Circumpolar Current. *Deep-Sea Research Part I*, *42*, 641–673. https://doi.org/10.1016/0967-0637(95)00021-w

Passow, U., & Carlson, C. (2012). The biological pump in a high CO_2 world. *Marine Ecology Progress Series*, *470*, 249–271. https://doi.org/10.3354/meps09985

Redfield, A. C. (1934). On the proportions of organic derivatives in sea water and their relation to the composition of plankton. *James Johnstone Memorial Volume* (pp. 176–192). Liverpool, UK: Liverpool University Press.

Riser, S. C., Swift, D., & Drucker, R. (2018). Profiling floats in SOCCOM: Technical capabilities for studying the Southern Ocean. *Journal of Geophysical Research: Oceans*, *123*, 4055–4073. https://doi.org/10.1002/2017JC013419

Roemmich, D., Church, J., Gilson, J., Monselesan, D., Sutton, P., & Wijffels, S. (2015). Unabated planetary warming and its ocean structure since 2006. *Nature Climate Change*, *5*, 240–245. https://doi.org/10.1038/nclimate2513

Sallée, J.-B., Pellichero, V., Akhoudas, C., Pauthenet, E., Vignes, L., Schmidtko, S., et al. (2021). Summertime increases in upper-ocean stratification and mixed-layer depth. *Nature*, *591*, 592–598. https://doi.org/10.1038/s41586-021-03303-x

Sambrotto, R. N., Savidge, G., Robinson, C., Boyd, P., Takahashi, T., Karl, D. M., et al. (1993). Elevated consumption of carbon relative to nitrogen in the surface ocean. *Nature*, *363*, 248–250. https://doi.org/10.1038/363248a0

Shadwick, E. H., Trull, T. W., Tilbrook, B., Sutton, A. J., Schulz, E., & Sabine, C. L. (2015). Seasonality of biological and physical controls on surface ocean CO_2 from hourly observations at the Southern Ocean Time Series site south of Australia. *Global Biogeochemical Cycles*, *29*, 223–238. https://doi.org/10.1002/2014GB004906

Shi, J.-R., Talley, L. D., Xie, S.-P., Peng, Q., & Liu, W. (2021). Ocean warming and accelerating Southern Ocean zonal flow. *Nature Climate Change*, *11*(12), 1090–1097. https://doi.org/10.1038/s41558-021-01212-5

Swart, N. C., & Fyfe, J. (2012). Observed and simulated changes in the Southern Hemisphere surface westerly wind-stress. *Geophysical Research Letters*, *39*, L16711. https://doi.org/10.1029/2012GL052810

Swart, N. C., Gille, S. T., Fyfe, J. C., & Gillett, N. P. (2018). Recent Southern Ocean warming and freshening driven by greenhouse gas emissions and ozone depletion. *Nature Geoscience*, *11*, 836–841. https://doi.org/10.1038/s41561-018-0226-1

Sweeney, C., Smith, W. O., Hales, B., Bidigare, R. R., Carlson, C. A., Codispoti, L., et al. (2000). Nutrient and carbon removal ratios and fluxes in the Ross Sea. *Antarctica.Deep Sea Research Part II*, *47*(15–16), 3395–3421. https://doi.org/10.1016/s0967-0645(00)00073-4

Szul, M. J., Dearth, S. P., Campagna, S. R., & Zinser, E. R. (2019). Carbon fate and flux in *Prochlorococcus* under nitrogen limitation. *mSystems*, *4*, e00254-18. https://doi.org/10.1128/msystems.00204-19

21699291, 2022, 9, Downloaded from https://agupubs.onlinelibrary.wiley.com/doi/10.1029/2022JC018859 by Noaa Department Of Commerce, Wiley Online Library on [21/04/2023]. See the Terms and Conditions (https://onlinelibrary.wiley.com/terms-and-conditions) on Wiley Online Library for rules of use; OA articles are governed by the applicable Creative Commons License

Takahashi, T., Broecker, W. S., & Langer, S. (1985). Redfield ratio based on chemical data from isopycnal surfaces. *Journal of Geophysical Research*, *90*, 6907–6924. https://doi.org/10.1029/jc090ic04p06907

Takahashi, T., Sutherland, S. C., Chipman, D. W., Goddard, J. G., & Ho, C. (2014). Climatological distributions of pH, pCO_2, total CO_2, alkalinity, and $CaCO_3$ saturation in the global surface ocean, and temporal changes at selected locations. *Marine Chemistry*, *164*, 95–125. https://doi.org/10.1016/j.marchem.2014.06.004

Talley, L. D., Feely, R. A., Sloyan, B. M., Wanninkhof, R., Baringer, M. O., Bullister, J. L., et al. (2016). Changes in ocean heat, carbon content, and ventilation: A review of the first decade of GO-SHIP global repeat hydrography. *Annual Review of Marine Science*, *8*(1), 185–215. https://doi.org/10.1146/annurev-marine-052915-100829

Toggweiler, J. R. (1993). Carbon overconsumption. *Nature*, *363*, 210–211. https://doi.org/10.1038/363210a0

Toggweiler, J. R., & Russell, J. (2008). Ocean circulation in a warming climate. *Nature*, *451*(7176), 286. https://doi.org/10.1038/nature06590

Verdy, A., & Mazloff, M. R. (2017). A data assimilating model for estimating Southern Ocean biogeochemistry. *Journal of Geophysical Research: Oceans*, *122*, 6968–6988. https://doi.org/10.1002/2016JC012650

Wanninkhof, R., Johnson, K., Williams, N., Sarmiento, J., Riser, S., Briggs, E., et al. (2016). *An evaluation of pH and NO_3 sensor data from SOCCOM floats and their utilization to develop ocean inorganic carbon products: A summary of discussions and recommendations of the Carbon Working Group (CWG) of SOCCOM*. Princeton, NJ: Princeton Environmental Institute.

Williams, N. L., Juranek, L. W., Feely, R. A., Johnson, K. S., Sarmiento, J. L., Talley, L. D., et al. (2017). Calculating surface ocean pCO_2 from biogeochemical Argo floats equipped with pH: An uncertainty analysis. *Global Biogeochemical Cycles*, *31*, 591–604. https://doi.org/10.1002/2016GB005541

Williams, N. L., Juranek, L. W., Feely, R. A., Russell, J. L., Johnson, K. S., & Hales, B. (2018). Assessment of the carbonate chemistry seasonal cycles in the Southern Ocean from persistent observational platforms. *Journal of Geophysical Research: Oceans*, *123*, 1–20. https://doi.org/10.1029/2017JC012917

Woosley, R. J., Millero, F. J., & Takahashi, T. (2017). Internal consistency of the inorganic carbon system in the Arctic Ocean. *Limnology and Oceanography: Methods*, *15*(10), 887–896. https://doi.org/10.1002/lom3.10208

21699291, 2022, 9, Downloaded from https://agupubs.onlinelibrary.wiley.com/doi/10.1029/2022JC018859 by Noaa Department Of Commerce, Wiley Online Library on [21/04/2023]. See the Terms and Conditions (https://onlinelibrary.wiley.com/terms-and-conditions) on Wiley Online Library for rules of use; OA articles are governed by the applicable Creative Commons License